ARTICLE IN PRESS

Available online at www.sciencedirect.com

SCIENCE DIRECT®

Biomaterials ▮ (▮▮▮▮) ▮▮▮–▮▮▮

Biomaterials

www.elsevier.com/locate/biomaterials

Synchrotron X-ray microtomography (on a micron scale) provides three-dimensional imaging representation of bone ingrowth in calcium phosphate biomaterials

P. Weiss[a,*], L. Obadia[a], D. Magne[a], X. Bourges[a], C. Rau[b], T. Weitkamp[b], I. Khairoun[a], J.M. Bouler[a], D. Chappard[c], O. Gauthier[a,d], G. Daculsi[a]

[a] *Laboratoire de Recherche sur les Matériaux d'Intérêt Biologique INSERM 99-03, Faculté de Chirurgie Dentaire, 1, place Alexis Ricordeau, 44042 Nantes cedex 01, France*

[b] *European Synchrotron Research Facility (ESRF), BP 220, 38043 Grenoble cedex, France*

[c] *LHEA Laboratoire Histologie-Embryologie, Faculté de Médecine, 49045 ANGERS cedex, France*

[d] *Laboratoire de Chirurgie, Ecole Nationale Vétérinaire de Nantes, Route de Gachet, BP 40706, 44307 Nantes cedex 03, France*

Received 16 December 2002; accepted 2 May 2003

Abstract

This study used synchrotron X-ray microtomography on a micron scale to compare three-dimensional (3D) bone ingrowth after implantation of various calcium phosphate bone substitutes in a rabbit model. The advantage of using this new method for the study of biomaterials was then compared with histomorphometry for analysis of interconnection and bone ingrowth. The study focused on the newly formed bone-biomaterial interface. Macroporous Biphasic Calcium Phosphate (MBCP™) ceramic blocks and two different injectable calcium phosphate biomaterials [an injectable bone substitute (IBS) consisting of a biphasic calcium phosphate granule suspension in hydrosoluble polymer and a calcium phosphate cement material (CPC)] were studied after in vivo implantation.

Absorption or phase-contrast microtomography was performed with the dedicated set-up at beamline ID22. Experimental spatial resolution was between 1 and 1.4 μm, depending on experimental radiation. All calcium phosphates tested showed osteoconduction. IBS observations after 3D reconstruction showed interconnected bioactive biomaterial with total open macroporosity and complete bone ingrowth as early as 3 weeks after implantation. This experimentation was consistent with two-dimensional histomorphometric analysis, which confirmed its suitability for biomaterials. This 3D study relates the different types of bone substitution to biomaterial architecture. As porosity and interconnection increase, bone ingrowth becomes greater at the expense of the bone substitute: IBS > MBCP > CPC.

Keywords: Microtomography; Synchrotron radiation; Calcium phosphate; Bone cement; Ceramics

1. Introduction

Calcium phosphate (CaP) biomaterials have been used for more than 15 years [1] in very different clinical applications such as repair of bone defects [2], bone augmentation in spinal arthrodesis [3,4], periodontal treatment [5], or coatings for metal implants [6]. They are also used as osteoconductive fillers to achieve coalescence with bone [7–9]. More recently, new percutaneous techniques have been developed in orthopedic surgery and especially in spinal surgery. Acrylic cementation of vertebrae [10] and filling of bone cysts [11] were the first documented applications.

However, numerous types of bone and dental surgery require bone substitutes. Injectable CaP biomaterials should associate efficient bone colonization and implantation with non-invasive surgical techniques. Two types of injectable bone substitutes (IBS) are presently under development in laboratories. Self-setting calcium phosphate cements (CPC) were the first bone substitutes developed [12] for percutaneous applications. These mineral hydraulic cements are not ready-to-use and require extemporaneous mixing, with various setting

*Corresponding author. Fax: +33-2-40-08-37-12.
E-mail address: pweiss@sante.univ-nantes.fr (P. Weiss).

0142-9612/03/$ - see front matter © 2003 Elsevier Ltd. All rights reserved.
doi:10.1016/S0142-9612(03)00335-1

and hardening times in situ [13–15]. CPC, after hardening, provides a dense ceramic with irregular gas microporosity [16], whereas numerous studies have shown the need for macropores to facilitate bone osteoconduction [17,18]. The second type of IBS, consisting of CaP ceramic granule suspensions in a water-soluble polymer carrier phase, was developed in our laboratory [19]. This IBS is ready-to-use, but has no initial mechanical properties. Bone ingrowth in the suspension is very rapid [20], and CaP granules in the polymer carrier phase create a so-called ''interconnected macroporosity'' [21].

The purpose of the present study was to compare the three-dimensional (3D) representation of bone ingrowth after implantation of two IBSs with that of biphasic CaP (BCP) macroporous blocks in a rabbit model [20–24], using synchrotron X-ray microtomography, a technique not previously applied to biomaterials. This imaging technique allows non-destructive 3D representation (with 1 μm resolution) of embedded calcified tissues, but has not yet been used to describe the bone substitution mechanism in vivo. The advantage of this new method for the study of biomaterials was then compared with classical histomorphometry for analysis of interconnection and bone ingrowth.

2. Materials and methods

2.1. Biomaterial preparation

2.1.1. BCP blocks

The BCP blocks used were Macroporous Biphasic Calcium Phosphate ceramic (MBCP™, Biomatlante, Vigneux, France) with a 60/40 HA/βTCP (w/w) ratio. All implants had macropore diameters of 300–565 μm, with 40–50% macroporosity. Biphasic structure and ceramic purity, as checked respectively by X-ray diffraction and Fourier transform infrared (FTIR) spectroscopy, confirmed the HA/βTCP ratio and the absence of carbonate and pyrophosphate impurities. Macro- and microporosity were determined by image analysis using scanning electron microscopy (SEM) observations. Microporosity was equivalent in all implants, representing 33% ± 0.5 of the ceramic surface [22]. Total micro- and macroporosity was 70%.

2.1.2. Injectable bone substitute

A CaP aqueous suspension was developed to obtain an injectable biomaterial associating a biphasic CaP ceramic mineral phase (MBCP®, Biomatlante, Vigneux, France) sieved in two different ranges (BCP granules 40–80, or 80–200 μm in diameter) with a 3% aqueous solution of a cellulosic polymer (hydroxypropylmethylcelullose) [25,26] in a 50/50 (w/w) ratio. The CaP fillers used were composed of BCP ceramic (60% HA and 40% β-tricalcium phosphate). The IBS was sterile, ready-to-use and injectable (CNRS Patent WO 95/21634; (MBCP Gel®)Biomatlante, Vigneux, France).

2.2. Bone cement

The CaP cement tested (CPC) consisted mainly of α-TCP and DCPA associated with smaller amounts of precipitated apatite and calcium carbonate ($CaCO_3$) [24]. Liquid and powder were mixed to form a paste that set in 6 min. The bone cement was prepared extemporaneously in sterile conditions prior to physical characterization and implantation in vivo.

2.2.1. In vivo study

The tested materials were implanted for 2, 3, 8 and 12 weeks into critical-sized bone defects at the distal end of rabbit femura. Implantations were performed on New Zealand white rabbits, as detailed in previous studies [20–24], in aseptic conditions and under general anesthesia. A 10 mm-long, 6 mm-diameter cylindrical defect was created at the distal end of the femur.

After the indicated implantation times, femoral ends were harvested from animals, and non-decalcified bone specimens were fixed in formol solution, successively dehydrated in graded ethanol and acetone and eventually infiltrated and embedded in methylmethacrylate with glycol. Only 1 sample for each implantation time and each biomaterial, treated in the previous studies, was used for this ESRF experimentation. For each sample, rods (0.6 mm × 0.6 mm × 10 mm) were cut perpendicularly to the drilling axis of the implantation site, using an Isomet™ diamond saw (Buehler LTD, Germany). Only a single sample from one animal at a time and of each biomaterial was used.

2.3. ESRF analysis

The experiment was carried out at the European Synchrotron Radiation Facility (ESRF, Grenoble, France) using microfluorescence, imaging and diffraction beamline ID22. High-energy electrons were produced in an accelerator and then circulated in a storage ring. When these electrons are deflected by strong magnetic fields, they emit electromagnetic waves referred to as synchrotron radiation. The light produced by a storage ring takes the form of a narrow and very intense beam, similar to that from a laser. Synchrotron radiation provides a monochromatic, high-photon flux X-ray beam. In conventional radiography, X-rays pass through the investigated object, and the transmitted intensity is recorded as a two-dimensional (2D) image. The information contained in this radiograph is a projection of the absorption density in the sample onto the plane perpendicular to the direction of the X-ray beam. With coherent illumination, the image also

contains information on the refractive index of the sample, which is apparent in what is known as phase contrast. If the sample is then imaged several times in different orientations, 3D (volume) information on the sample structure can be obtained using computer algorithms. This process, referred to as *tomographic reconstruction* or *tomography*, allows slices of the investigated object to be observed without physically cutting it. Fig. 1 shows the experimental scheme of the microtomography endstation at undulator beamline ID22 at the ESRF.

Synchrotron electron current is 200 mA, and source size at the high-beta section is $800\,\mu m \times 30\,\mu m$ (FWHM). The undulator (38 magnetic periods; period length: 42 mm) produces an X-ray spectrum with a series of intensity spikes. The integral flux over the whole energy spectrum is about 10^{15} photons/s mm^2. The typical energy width $\Delta E/E$ of one undulator harmonic is about 10^{-2}. The polychromatic beam is deflected by a single crystal silicon mirror with different coatings in order to suppress higher harmonics. The platinum strip at a deflection angle of $\alpha = 0.15^\circ$ defines the cut-off energy of 32 keV. For further limitation of the energy bandwidth, a conventional double-crystal fixed-exit Si-111 monochromator with an energy bandwidth of $\Delta E/E \sim 10^{-4}$ at 20 keV is used. All X-ray optical elements are kept under vacuum.

In our study, the sample was mounted at a distance of 65 m from the undulator source, and the rotation axis was horizontal. A detailed description of the tomography stage can be found elsewhere [27,28]. The distance between sample stage and detector can be freely chosen in order to increase phase contrast by using highly coherent light from the third-generation synchrotron radiation source as it is in ESRF. Phase contrast imaging and tomography are especially well suited for poorly absorbing biological samples with low absorption contrast. The distance between the sample and the detector was between 2 and 10 mm, as only features with low absorption contrast can be revealed at greater distances. Moreover, high X-ray energies allowed radiation damage to the sample to be reduced.

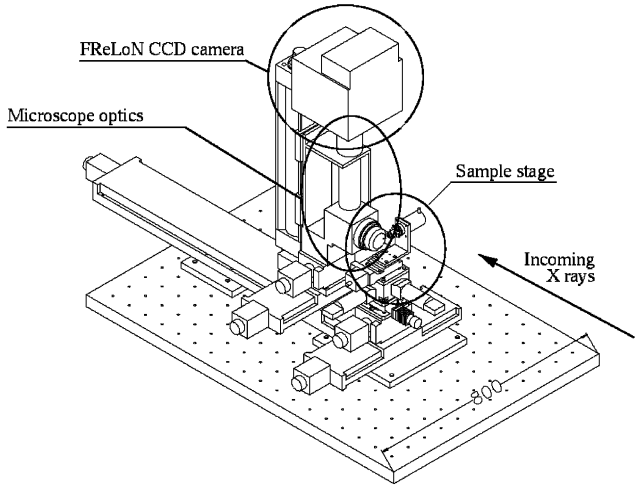

Fig. 1. The microtomographic stage at ID 22 (measurements in millimeters). A sample stage (foreground) and detector system (behind) consisting of a visible-light microscope with a three-objective revolver magnifying the scintillation image from a doped YAG or LAG single-crystal screen, and a FreLon 2000 CCD camera. Sample-to-scintillator distance can be set from less than 1 mm (as shown in the figure) to almost 1 m, thereby allowing both absorption-contrast and phase-contrast imaging in different regions of wavefront propagation. The rotation axis is horizontal because of the higher degree of beam coherence in the vertical direction, yielding more phase contrast in that dimension.

In the CCD-based high-resolution X-ray image detectors commonly used in microtomography, a visible-light image is generated by a fluorescent screen and then projected by a photon microscope onto a CCD camera. The resolution of such a system is between 1 and 3 μm[1] depending on the scintillator screen and optical magnification chosen.

The shadow projections of the object were recorded with a high-resolution CCD-based camera system [28], which operates on the principle of converting incident X-ray photons to visible light with a scintillator screen and then magnifying the image with microscope optics on a CCD system. A light microscope with interchangeable objectives, allowing magnifications $\times 10$, 20 or 40, projected the scintillation-light image onto a 2048×2048-pixel CCD camera with a 14-bit real dynamic range. As the size of a single CCD $\times$ pixel is 14 μm, the image on the scintillator screen can be (over-)sampled with an effective pixel size down to $0.35\,\mu m \times 0.35\,\mu m$. However, smaller optical magnifications and binning of the pixel on CCD chips allow a significant reduction in the amount of data to be treated. For each tomographic procedure, 625 projection images were taken over an angular range of 180°. Exposure times per projection ranged between 3 and 10 s. For our experiments, the scintillator was a lutetium aluminum garnet (LAG) single crystal with a 12 μm-thick europium-doped luminescent layer. A light microscope (magnification: $\times 10$) projected the scintillation-light image onto a 2048×2048-pixel CCD camera with a 14-bit real dynamic range. For this configuration, effective pixel size was 1.4 μm, corresponding to the resolution of the chosen scintillation screen. After dark field correction and flat field normalization of the projections, single slices perpendicular to the rotation axis were reconstructed with the filtered back-projection technique [29]. For reconstruction, "HST," an ESRF-developed program, was used. Using a complete set of reconstructed slices, a volume image of the studied sample was generated. The different features of the sample were selected by sectioning the different gray levels of the low-noise data.

2.4. Histomorphometry

2D (6–8 slices in TIFF format imaging) histomorphometric analysis was performed on a Leica Quantimet Q570 image processor. This analyzer can store 24 gray images coded on 8 bits and 24 binary images, and five colored bitplanes are used as overlays. Numerous mathematical morphology functions are available through an image-oriented language derived from Microsoft QBasic housed in a PC-compatible 486. Six to eight randomized tomographic slides for each sample were transformed to 512×512 pixel images. After interactive thresholding, a binary image of the bony component was obtained. Only mineralized or unmineralized information was available after binaryzation. Several algorithms have been described elsewhere to quantify the trabecular bone architecture on semi-serial histological section [30]. The method was also found adequate to describe the architecture of porous biomaterials when applied to semi-serial sections provided by X-ray microtomography [31].

3D histomorphometric analysis was performed in voxels with Imaris™ (Bitplane AG, Zurich, Switzerland) software.

3. Results

Two examples of these slides generated from IBS implantations (Fig. 2) indicate that the BCP granules were embedded in mineralized bone matrix. Bone ingrowth was abundant and similar to that obtained in previous studies with SEM using backscattered electrons [20,22,23]. Concentric circles, visible in all slices, were due to temporal modulation of the illumination with the X-ray beam during the tomographic scan. Many small cavities were visible, which probably represented osteocytic *lacunae* (osteoplasts), and larger unmineralized soft tissue spaces (presumably closed in 2D representation) were present between mineral walls.

3D representation (Fig. 3) of physiological trabecular rabbit bone shows the usual architectural bone structures, with numerous osteoplasts (osteocyte *lacunae*) (A), many interconnected tubes that appear to be vascular canals (B) of bone, and large marrow spaces between bone trabeculae (C).

The results obtained with MBCP blocks (Fig. 4) show osseointegration of CaP ceramics in peripheral areas. Bone in contact with MBCP blocks appears to be physiological lamellar bone, with osteons, vascular canals and many osteoplasts (A). The osteoconduction mechanism occurs homogeneously at the ceramic surface and in peripheral macropores (A, B). In fact, 10% of BCP ceramics were resorbed between 3 and 8 weeks of implantation in the peripheral area (Table 1). Macropores show interconnections in peripheral implant areas, but seem to be unconnected in the center of the BCP implant (C). In fact, no bone ingrowth occurred after 3 weeks of implantation in the center of BCP blocks.

The images (Fig. 5) obtained for the IBS with small BCP granules (40–80 μm) show bone ingrowth progressing from one granule to another in the peripheral area, with no isolated granules (A). Bone is in close contact with BCP granules and with many osteoplasts. Large spaces without mineral are visible. No newly formed bone was detected in the center of this implant after 2 weeks (B).

Three weeks after implantation, tomographic 3D images of the center of the implant [IBS 40–80μm; Fig. 6 (A)] revealed intense bone ingrowth, with very little soft tissue or empty space remaining (apparently

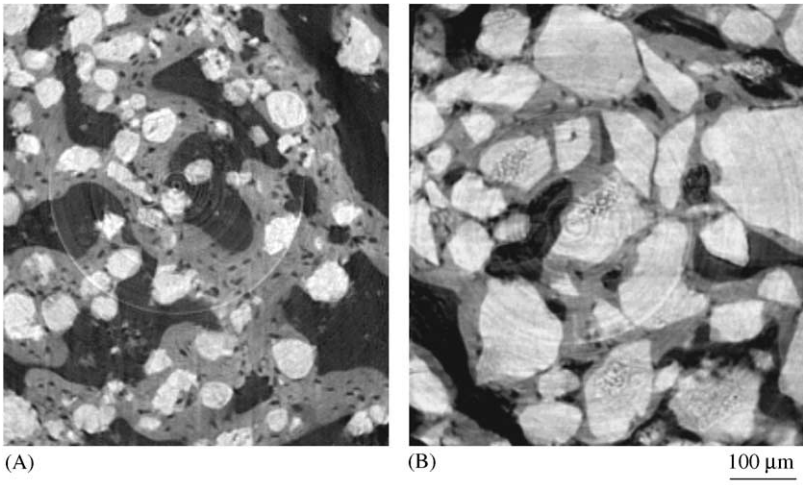

Fig. 2. Tomographic 2D reconstructed section of the rods perpendicular to the long axis. Bone in gray, BCP granules in white, and soft tissue in black: (A) IBS 40–80 μm after 3 weeks of implantation into a rabbit model and (B) IBS 80–200 μm after 3 weeks of implantation into a rabbit model.

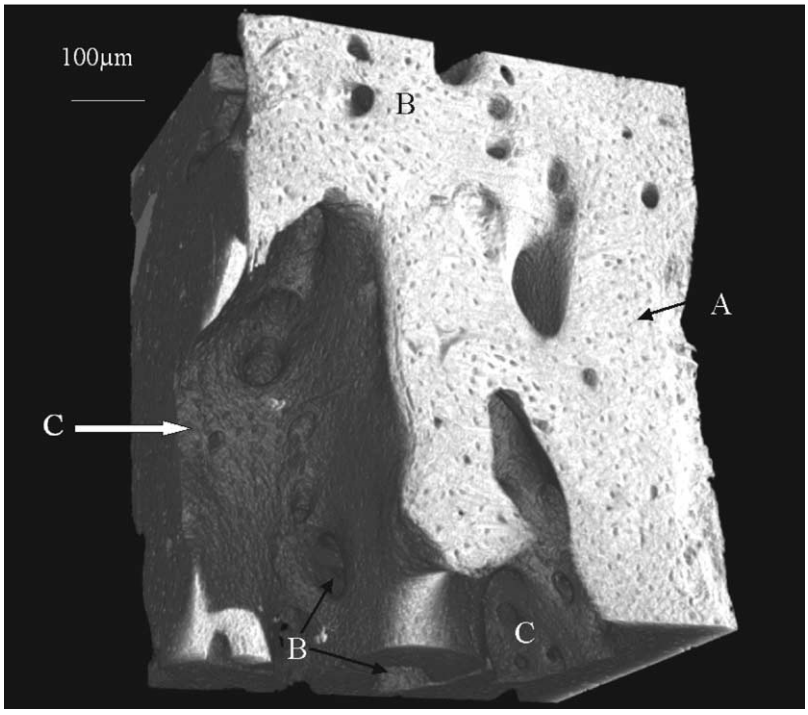

Fig. 3. Tomographic 3D representation of trabecular rabbit bone near implanted biomaterial: (A) Osteoplasts (osteocyte *lacunae*), (B) vascular canals and (C) large soft tissue areas.

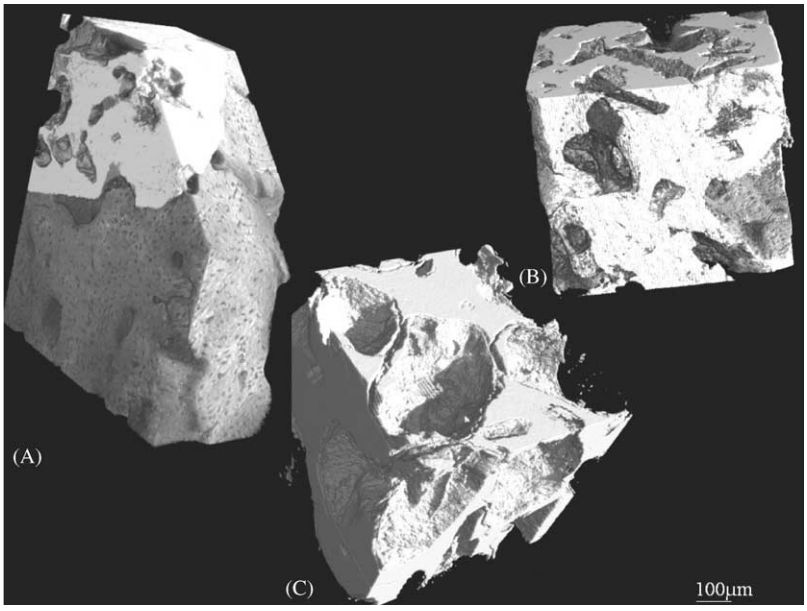

Fig. 4. Tomographic 3D representation of BCP blocks implanted into rabbit bone after 8 weeks: (A) Superficial area of BCP with 300 μm macropores 8 weeks after implantation, (B) CP blocks with 400–600 μm macropores 8 weeks after implantation and (C) center of BCP blocks with 400–600 μm macropores 3 weeks after implantation.

less than in control bone without IBS). After 8 weeks of implantation, the peripheral implant (B) was more representative of physiological bone, with large interconnected soft tissue spaces and trabecular areas.

The percentages of mineral phase (BCP granules and newly formed bone) were well correlated between quantitative 3D and 2D results ($r^2 = 0.75$) (Tables 1 and 2).

The bone volume/total volume ratio (BV/TV) increased with time, reaching a maximum at 3 weeks of implantation (Table 1) and showing increasing trabecular thickness (Tb.Th) (Table 2). The resorption

process started earlier, as soon as 2 weeks on the border and in the middle (zone between the center and the border) areas of the implant (14–16%). In the center, this value was reached at 8 weeks (Table 1). The organic or "empty" spaces were very small (26%) in the center of the implant after 3 weeks, but later reverted to earlier values (44%).

2D histomorphometric measurements revealed the following (Table 2):

- A minimal interconnection index (ICI) at 3 weeks, prior to an increase at 8 weeks.
- A maximum free end count at 2 weeks.
- Maximum node to node (NNS) and minimum node to free at 3 weeks.
- A decrease in marrow star volume prior to an increase at 3 weeks ($\times 5$).
- Marrow star volume was always lower in the center.
- An increase in trabecular star volume at 2 weeks.

Table 1
3D (voxel) ratio measurements of mineral phases (BCP/bone) with different calcium phosphate biomaterials implantation in rabbit model

Sample, situation, implantation time	BCP (%)	Bone (BV/TV) (%)
BCP 400–600, border, 3 weeks	33	32
BCP 400–600, border, 8 weeks	24	34
IBS 40–80, border, 2 weeks	14	38
IBS 40–80, medium, 2 weeks	16	41
IBS 40–80, center, 2 weeks	31	0
IBS 40–80, border, 3 weeks	13	47
IBS 40–80, center, 3 weeks	29	45
IBS 40–80, border 8 weeks	15	42
IBS 40–80, center 8 weeks	14	42
IBS 80–200 suspension before implantation	28	0
IBS 80–200, border 3 weeks	26	31
IBS 80–200, center 3 weeks	36	34

3D imaging of an IBS with small BCP granules (80–200 μm granules) (Fig. 7) shows high amounts of bone ingrowth and very few soft tissue spaces after 3 weeks of implantation in the center of the surgical implantation site (A). On the periphery of the defect (B), the implant is more representative of physiological bone, with large interconnected soft tissue areas similar to those observed in trabecular bone. 3D measurements (Table 1) showed a very high mineral phase level in the center of the implant, similar to that of IBS 40–80 for the same time interval, with a low rate of organic or empty phases. In contrast to IBS 40–80, bone ingrowth was lower in IBS 80–200, with little resorption. 2D histomorphometric measurements showed considerable trabecular thickness in the center, with a high trabecular star volume level. In all IBS images, all granules were totally surrounded by bone mineral tissue.

The tomographic study of CPC revealed a different way of bone integration (Fig. 8). The surface of the CPC implant (A) seems to be very tortuous and covered by a uniform thin layer of bone. Osteoconduction was observed early on the cement surface, but bone ingrowth only occurred in small fissures or defects on the surface of the implant (B). Tomographic slices of the center of the implant showed no bone formation after 3 weeks of implantation (C).

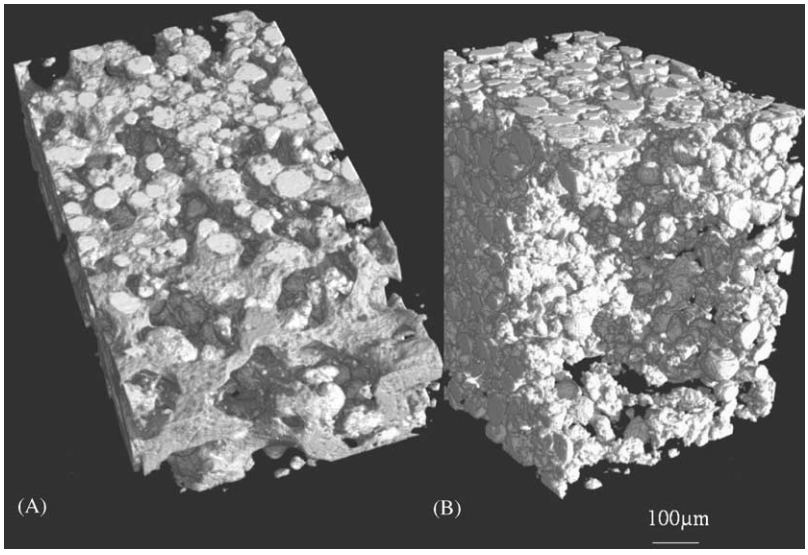

Fig. 5. Tomographic 3D representation of IBS formulated with BCP granules sieved between 40 and 80 μm and implanted into rabbit bone for 2 weeks: (A) Superficial area of IBS and (B) center of the IBS implant.

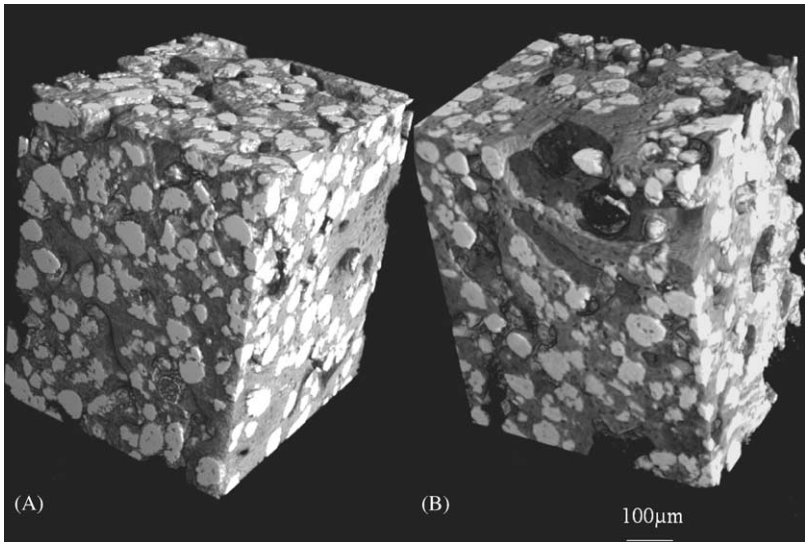

Fig. 6. Tomographic 3D representation of IBS formulated with BCP granules sieved between 40 and 80 μm and implanted into rabbit bone: (A) Center of the IBS implant after 3 weeks of implantation and (B) center of the IBS implant after 8 weeks of implantation.

Table 2
2D (pixel) ratio measurements of mineral phases and histomorphometric data with different calcium phosphate biomaterials implantation in rabbit model

Sample, situation, implantation time	Mineral phase (%)	Tb Th(μm)	ICI	FEC	NC	NNS	NFS	FFS	Marrow star volume	Trabecular star volume
IBS 40–80 border at 2 weeks	47.97	155	1.05	15.96	20.44	56.56	26.12	1.57	0.74	0.35
IBS 40–80 middle at 2 weeks	48.24	143	1.27	20.58	27.61	57.71	24.03	1.11	0.60	0.26
IBS 40–80 border at 3 weeks	58.58	179	0.94	12.33	24.33	66.88	17.53	0.54	0.32	0.68
IBS 40–80 center at 3 weeks	73.29	260	0.90	12.13	19.86	65.10	19.93	0.48	0.12	1.60
IBS 40–80 border at 8 weeks	57.00	238	1.22	10.84	17.41	64.49	18.64	0.57	1.42	1.40
IBS 40–80 center at 8 weeks	61.77	205	1.18	12.45	23.24	67.15	17.16	0.90	0.55	1.11
IBS 80–200 border at 3 weeks	60.21	196	1.39	13.94	16.16	56.35	25.00	2.25	0.38	0.95
IBS 80–200 center at 3 weeks	80.11	376	1.05	8.73	12.09	56.65	29.86	0.28	0.13	10.56

Mineral phase % (BCP volume + Bone volume/Total Volume), Tb Th: trabecular thickness, ICI: interconnected index, FEC: free end count, NC: node count, NNS: node to node (%), NFS: node to free end (%), FFS: free end to free end (%).

All CaP materials tested showed total surface osteoconduction, with different degrees of penetration inside the CaP implants. CPC surface was totally in contact with both host bone and peripheral external new bone, but bone ingrowth was superficial and occurred only in surface fissures, without any colonization of the implant body. MBCP blocks showed better bone colonization in superficial macropores, but in the early steps of substitution (3–8 weeks) the center of the implant showed no bone colonization because of the poor interconnection level of the BCP blocks. After the third week of implantation, the whole IBS suspension implant was uniformly colonized by newly formed bone and there were few remaining empty spaces. After 8 weeks, trabecular bone structure was still visible.

4. Discussion

The main limitation of the synchrotron X-ray microtomography technique used here is sample size. The sample must measure less than 1 mm^3 because of the size of the X-ray beam, thus making it difficult to analyze the whole implantation area. For this first study, a configuration for high definition was used and for each sample acquisition, transfer and treatment data was about several hours. For one weeks of experimentation, only 20 samples were correctly treated with a good result. It is difficult to study completely one sample for quantitative study and to repeat the same experiment 3 times with 3 different samples from different animals for the reproductibility of the results. Another technique

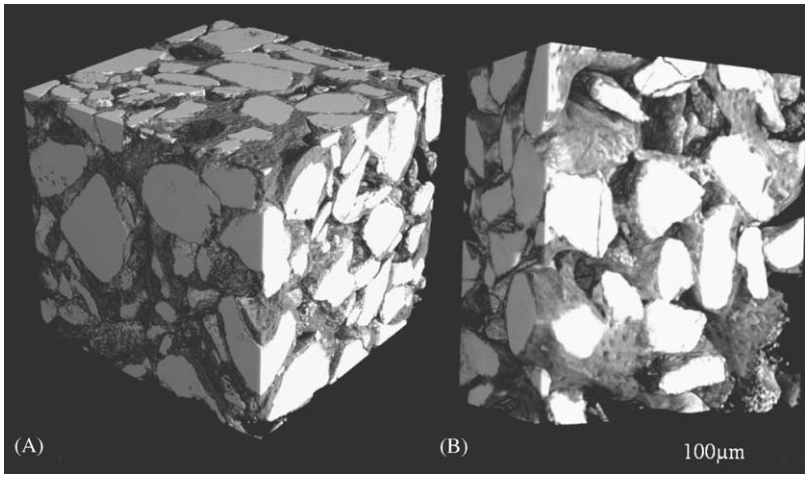

Fig. 7. Tomographic 3D representation of IBS formulated with BCP granules sieved between 80 and 200 μm and implanted into rabbit bone: (A) Center of the IBS implant after 3 weeks of implantation and (B) border of the IBS implant after 3 weeks of implantation.

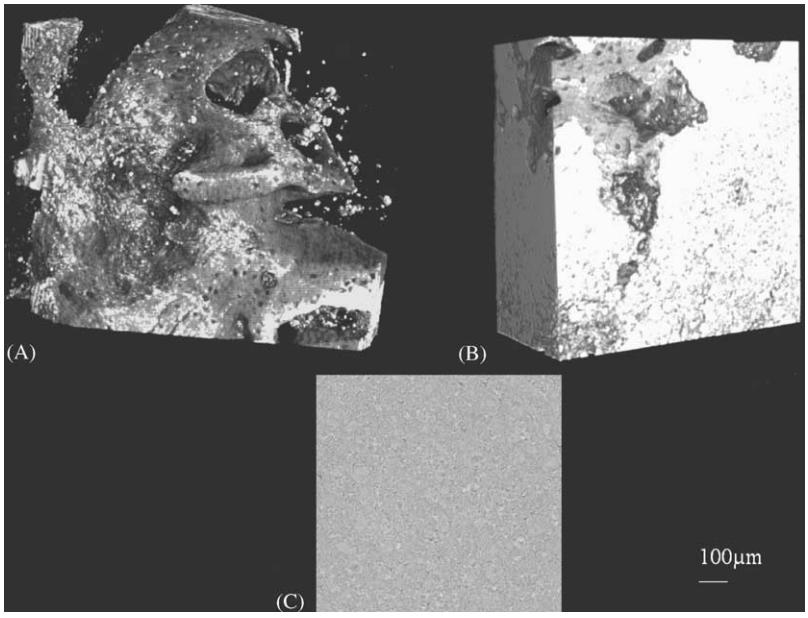

Fig. 8. Tomographic 3D representation of calcium phosphate cement implanted into rabbit bone for 3 weeks: (A) Surface of CPC implant, (B) border of CPC implant and (C) tomographic slice from the center of the CPC after implantation.

developed at the ESRF in ID 19, allows analysis of larger samples (4 mm × 4 mm × 4 mm), with spatial resolution between 9 and 15 μm. However, the results obtained [32] do not provide enough details to describe the bone-biomaterial interface precisely, and in any case sample size is still limited. Yet this technique may be useful for studying general ingrowth architecture and comparing these 3D images with the findings for other microtomodensitometric methods based on laboratory X-ray sources [33,34]. The latter methods are less costly, but provide poorer spatial resolution and definition. Only synchrotron radiation with monochromaticity, high coherence and photon flux allows spatial resolution of about 1 μm. The monocrystal size and the micropores of CaP ceramic are usually about 1 μm. Thus, phase-contrast microtomography is an interesting method for comparing both biomaterial reactions at this scale with high resolution and high contrast. SEM does not allow volume analysis, and slice preparation can modify the structure of the bone-biomaterial interface. 2D description of one slice is not sufficient to represent the connectivity between two spaces. The results in Fig. 2 are similar to those obtained with SEM [20,23,35], but provide no information about 3D structure. It is impossible to know whether bone trabeculae are interconnected or not as physiological structures. For instance, with 2D description it is difficult to know how bone colonization occurs between two granules, whereas

3D representation shows that all CaP surfaces near bone tissue are rapidly covered with bone. The present study confirms the role of CaP materials as scaffolds and emphasizes the osteoconductive properties of CaP biomaterials [2,8,18,36]. Deposition of bone directly on the surface of the biomaterial is also confirmed, because a layer of bone was always present on all biomaterial surfaces, without any complete continuity between host bone and the biomaterial bone layer surface.

CPC is a massive material [16] without macroporosity that allows good osteoconductivity on its surface, but acts as a barrier to colonization inside the implant. Moreover, the surface (circumference and tiny peripheral fissures) accessible for cell action and the resorption process is minimal. As a result, cement degradation is limited and substitution is slow [26].

With BCP blocks, macroporosity increases the implant surface accessible for resorption. Both bone ingrowth onto the surface of macropores and the resorption process of the implant lead to interconnections from the surface to the center of the defect. Consecutive bone substitution is more efficient than with CPC, but bone apposition is still slow and highly influenced by the interconnection level of the initial macroporosity, as revealed by 3D microtomographic reconstruction (Fig. 4). Interconnection of BCP implants proved too limited to support fast extensive bone apposition.

After the third week of implantation, the whole implant area of IBS was uniformly colonized by newly formed bone and there were few remaining empty spaces. This confirms that the polymer, in water solution (2–3% w/w), was not a barrier. The IBS suspension before implantation can be considered, from a point of view of mineral phase, as an interconnected bioactive biomaterial with total open macroporosity, as indicated by 3D reconstruction.

However, with the IBS biomaterial, no new bone was visible in the center of the implant 2 weeks after implantation, even though body fluids, cells or proteins were easily diffused within the BCP particle network. Interconnection is necessary, but not sufficient by itself, to provide uniform bone colonization in the whole implant. Bone colonization could relate to the progression of the neovascular system, which gradually developed within the implant site from host bone tissue on the surface of the surgical site into the implant. After 3 weeks, the whole implant was colonized by a mineralized bone tissue network in the center of the implant, which had a higher density than physiological bone, while trabecular spaces again became visible in peripheral areas. After 8 weeks, marrow space volume increased again, and the architecture of the newly formed bone was more like that of host bone. 3D representations (Figs. 3–7), according to histomorphometric measurements (Tables 1 and 2), provide information about interconnectivity and physiological trabecular spaces, which suggests that the vascular system plays a role in biomaterial bone ingrowth (as in the bone shown in Fig. 3). At the beginning of bone ingrowth, mineral phase density (bone and BCP) was very high and in fact much higher than in physiological bone (peripheral IBS implant at 2 weeks or central IBS implant at 3 weeks). This very high bone ingrowth occurred only near physiological trabecular space and not everywhere in the implant at the same time. This suggests that bone progression inside the center of the interconnected biomaterials requires preliminary bone substitution to provide soft tissue areas that are able to carry cells and a new vascular system (peripheral IBS implants at 3 and 8 weeks).

The following process of bone ingrowth in IBS biomaterial seems likely:

- Protein adsorption, dissolution and precipitation of carbonated apatites occur on all surfaces of BCP granules [2].
- As confirmed in this study, bone formation near host bone occurs in two directions in the biomaterial, one from host bone toward the biomaterial and the other from the biomaterial toward host bone [37]: 3D images and quantitative data show that isolated mineral zones, BCP granules embedded in layer of bone, are not initially continuous and have little organization, high interconnection and a low bone level. No bone was present in the center of the IBS implant at 2 weeks.
- The mineral phase increases (BV/TV and Tb.Th increase) before resorption process near the vascular system of host bone.
- The neovascular system and resorption cells modify the architecture of the IBS by producing newly formed bone: BV/TV decreases after an initial increase phase. 3D representation showed marrow spaces on the border, with an increase in elements specific for the organizational level. The IBS with small granules had high contact surface for cells as compared to the IBS with larger fillers or to CaP biomaterials. BCP resorption was higher and bone ingrowth faster, in accordance with findings in a previous study [20].
- BV/TV is very high in front of this area and in the center of the implant, with a much lower level of organic phase spaces before the vascular and resorption processes.

Bone substitution progressed rapidly (like a wave) from host bone to the center of the IBS implant with a centripetric remodeling process (creeping substitution).

This study indicates the importance of biomaterial structure and architecture for bone colonization kinetics relative to the opposition between initial mechanical strength (CPC) and rapid substitution (IBS). IBS had no

early mechanical properties, but "physiological" bone formed after only 3 weeks of implantation in this rabbit model. However, CPC cements were not resorbed after the same period. CPC is a primary hardening biomaterial with a slow substitution rate, and IBS is a suspension with a fully mineral interconnected structure that can in fact restore bone structure, providing secondary early mechanical strength induced by bone ingrowth.

5. Conclusion

In conclusion, 3D microtomographic reconstruction allows evaluation of bone architecture with a resolution of 1 μm and shows the quality of bone ingrowth into various types of bone substitute implants. This method is very precise, allowing imaging of 3D reconstruction of bone growth by osteons and osteoplasts, but not general and quantitative measurements of entire implants. Although performed on a limited number of samples, this type of experimentation is in accordance with 2D histomorphometric analysis and confirms the use of the 3D microtomographic technique with biomaterials and its complementarity with the 2D method.

All CaPs tested showed total surface osteoconduction, with different degrees of penetration within the implant. Observations of IBS figures after 3D reconstruction showed an interconnected bioactive biomaterial with total open macroporosity and complete bone ingrowth after 3 weeks of implantation. This method confirms that 3D ingrowth of bone into IBS was better and more "physiological" than that of the other CaP biomaterials studied. This 3D study indicates the different types of bone substitution in relation to biomaterial architecture. As porosity and interconnection increase, bone ingrowth becomes greater at the expense of the bone substitute: IBS > MBCP > CPC.

Acknowledgements

This study was supported by the Pays de Loire Region (France) under a contract "plan Etat Région Biomatériaux 2000–2006," the European Synchrotron Research Facility (ESRF) and the European Union.

The authors acknowledge J. Guicheux for critically reading the manuscript and valuable comments, P. Pilet for technical assistance and S. Bohic for his help in the elaboration of the ESRF proposal.

References

[1] De Groot K. Bioceramics of calcium phosphate. Boca Raton, FL: CRC Press; 1983.
[2] Daculsi G, LeGeros RZ, Heughebaert M, Barbieux I. Formation of carbonate-apatite crystals after implantation of calcium phosphate ceramics. Calcif Tissue Int 1990;46:20–7.
[3] Passuti N, Daculsi G, Rogez JM, Martin S, Bainvel JV. Macroporous calcium phosphate ceramic performance in human spine fusion. Clin Orthop 1989;248:169–76.
[4] Cavagna R, Daculsi G, Bouler JM. Macroporous calcium phosphate ceramic: a prospective study of 106 cases in lumbar spinal fusion. J Long Term Eff Med Implants 1999;9:403–12.
[5] LeGeros RZ. Calcium phosphate materials in restorative dentistry: a review. Adv Dent Res 1988;2:164–80.
[6] Delecrin J, Daculsi G, Passuti N, Duquet B. Specific resorbable calcium phosphate coating to enhance osteoconduction. Cells Mater 1994;4:51–62.
[7] Daculsi G, LeGeros RZ, Nery E, Lynch K, Kerebel B. Transformation of biphasic calcium phosphate ceramics in vivo: ultrastructural and physicochemical characterization. J Biomed Mater Res 1989;23:883–94.
[8] Daculsi G, LeGeros RZ, Deudon C. Scanning and transmission electron microscopy, and electron probe analysis of the interface between implants and host bone. Osseo-coalescence versus osseointegration. Scanning Microsc 1990;4:309–14.
[9] Daculsi G, Bagot d'Arc M, Corlieu P, Gersdorff M. Macroporous biphasic calcium phosphate efficiency in mastoid cavity obliteration: experimental and clinical findings. Ann Otol Rhinol Laryngol 1992;101:669–74.
[10] Kaemmerlen P, Thiesse P, Jonas P, Berard CL, Duquesnel J, Bascoulergue Y, Lapras C. Percutaneous injection of orthopedic cement in metastatic vertebral lesions. N Engl J Med 1989;321:121.
[11] Adamsbaum C, Kalifa G, Seringe R, Dubousset J. Direct Ethibloc injection in benign bone cysts: preliminary report on four patients. Skeletal Radiol 1993;22:317–20.
[12] Drissens F, Bolton M, Bermudez O, Planell J, Ginebra M, Fernandez E. Effective formulation for the preparation of calcium phosphate hone cements. J Mater Sci 1994;5:164–70.
[13] Khairoun I, Boltong MG, Driessens FC, Planell JA. Effect of calcium carbonate on the compliance of an apatitic calcium phosphate bone cement. Biomaterials 1997;18:1535–9.
[14] Khairoun I, Boltong MG, Driessens FC, Planell JA. Effect of calcium carbonate on clinical compliance of apatitic calcium phosphate bone cement. J Biomed Mater Res 1997;38:356–60.
[15] Lemaitre J, Munting E, Mirtchi A. Setting, hardening and resorption of calcium phosphate hydraulic cements. Rev Stomatol Chir Maxillofac 1992;93:163–5.
[16] Constantz B, Ison I, Fulmer M, Poser R, Smith S, VanWagoner M, Ross J, Goldstein SA. Skeletal repair by in situ formation of the mineral phase of bone. Science 1995;267:1796–9.
[17] De Groot K. Bioceramics consisting of calcium phosphate salts. Biomaterials 1980;1:47–50.
[18] Daculsi G, Passuti N. Effect of the macroporosity for osseous substitution of calcium phosphate ceramics. Biomaterials 1990;11:86–7.
[19] Daculsi G, Weiss P, Delecrin J, Grimandi G, Passuti N. Biomaterial composition-preparation proceeding. International Patent: WO 95/21634, 1994.
[20] Gauthier O, Bouler JM, Weiss P, Bosco J, Daculsi G, Aguado E. Kinetic study of bone ingrowth and ceramic resorption associated with the implantation of different injectable calcium phosphate bone substitutes. J Biomed Mater Res 1999;47:28–35.
[21] Weiss P, Gauthier O, Bouler JM, Grimandi G, Daculsi G. Injectable bone substitute using a hydrophilic polymer. Bone 1999;25:67S–70S.
[22] Gauthier O, Bouler JM, Aguado E, Pilet P, Daculsi G. Macroporous biphasic calcium phosphate ceramics: influence of

macropore diameter and macroporosity percentage on bone ingrowth. Biomaterials 1998;19:133–9.
[23] Gauthier O, Bouler JM, Weiss P, Bosco J, Aguado E, Daculsi G. Short-term effects of mineral particle sizes on cellular degradation activity after implantation of injectable calcium phosphate biomaterials and the consequences for bone substitution. Bone 1999;25:71S–4S.
[24] Khairoun I, Magne D, Gauthier O, Bouler JM, Aguado E, Daculsi G, Weiss P. In vitro characterization and in vivo properties of a carbonated apatite bone cement. J Biomed Mater Res 2002;60:633–42.
[25] Amouriq Y, Bourges X, Weiss P, Bosco J, Bouler JM, Daculsi G. Skin sensitisation study of two hydroxypropyl methylcellulose components (Benecel® and E4m®) of an injectable bone substitute in guinea pigs. J Mater Sci Mater Med 2002;13:149–54.
[26] Gauthier O, Khairoun I, Bosco J, Obadia L, Bourges X, Rau C, Magne D, Bouler JM, Aguado E, Daculsi G, Weiss P. Non-invasive bone replacement using a new injectable calcium phosphate biomaterial. J Biomed Mater Res, in press.
[27] Raven C. Microimaging and tomography with high-energy coherent synchrotron X-rays. Aachen: Shaker Verlag; 1998.
[28] Weitkamp T, Raven C, Snigirev A. In: Bonse U, editors. Developments in X-ray tomography II, SPIE Proceedings, vol. 3772, 1999. p. 311–7.
[29] Kak AC, Slaney M. Principles of computerized tomographic imaging. New York: IEEE Press; 1988.
[30] Chappard D, Legrand E, Pascaretti C, Basle MF, Audran M. Comparison of eight histomorphometric methods for measuring trabecular bone architecture by image analysis on histological sections. Microsc Res Technol 1999;45:303–12.
[31] Filmon R, Retailleau-gaborit N, Grizon F, Galloyer M, Cincu c, Basle MF, Audran M, Chappard D. Non-connected versus inter-connected macroporosity in poly (2-hydroxyethyl methacrylate) polymers. An X-ray microtomographic and histomorphometric study. J Biomater Sci Polym Ed 2002;13:1105–17.
[32] Salomé M, Peyrin F, Cloetens P, Odet C, Laval-Jeantet A-M, Baruchel J, Spanne P. A synchrotron radiation microtomography system for the analysis of trabecular bone samples. Med Phys 1999;26:2194–204.
[33] Pothuaud L, Van Rietbergen B, Mosekilde L, Beuf O, Levitz P, Benhamou CL, Majumdar S. Combination of topological parameters and bone volume fraction better predicts the mechanical properties of trabecular bone. J Biomech 2002;35:1091–9.
[34] Muller R, Van Campenhout H, Van Damme B, Van der Perre G, Dequeker J, Hildebrand T, Ruegsegger P. Morphometric analysis of human bone biopsies: a quantitative structural comparison of histological sections and micro-computed tomography. Bone 1998;23:59–66.
[35] Gauthier O, Bouler JM, LeGeros RZ, Agado E, Pilet P, Daculsi G. Elaboration conditions influence physicochemical properties: an in vivo bioactivity of macroporous biphasic calcium phosphate ceramics. J Mater Sci Mater Med 1999;10:199–204.
[36] Daculsi G, Passuti N, Martin S, Deudon C, Legeros RZ, Raher S. Macroporous calcium phosphate ceramic for long bone surgery in humans and dogs. Clinical histological study. J Biomed Mater Res 1990;24:379–96.
[37] Puleo DA, Nanci A. Understanding and controlling the bone-implant interface. Biomaterials 1999;20:2311–21.